The Impact of Microwave Absorber and Radome Geometries on Ground-Based GNSS Measurements of Coordinates and Atmospheric Water Vapour

T. Ning, G. Elgered, J.M. Johansson

Department of Radio and Space Science, Chalmers University of Technology

Onsala Space Observatory, SE-439 92 Onsala, Sweden

Abstract

We present results on the microwave absorbing material in different geometries around ground-based Global Navigation Satellite System (GNSS) antennas in order to mitigate multipath effects on the estimates of coordinates and atmospheric water vapour. The influence of the installation of a hemispheric radome on the antenna was also investigated. Two GNSS stations at the Onsala Space Observatory were used forming a 12 m baseline. Nearly one year of data starting from Oct. 2008, was analyzed by the GIPSY/OASIS II software using the Precise Point Positioning (PPP) processing strategy with the Niell Mapping Function (NMF), and for five different elevation cutoff angles from 5° to 25°. We found that the use of the absorbing material decreases the offset in the estimated vertical component of the baseline from ∼27 mm to ∼4 mm when the elevation cutoff angle varies from 5° to 20°. Two different configurations of the absorber give similar results with a mean difference less than 3 mm. The horizontal components are much less affected. The changes within 5 mm in the offsets in the vertical component of the baseline are seen for all five elevation cutoff angle solutions when the antenna was covered by a hemispheric radome. The offset, also from 5° to 20°, in the estimates of the atmospheric Integrated Water Vapour (IWV) decreases from ∼1.6 kg/m^2 to ∼0.3 kg/m^2. Using the radome affects the IWV estimates less than 0.4 kg/m^2 for all different solutions. IWV comparisons between a Water Vapour Radiometer (WVR) and the GPS data give consistent results.

Key words: GNSS antennas; multipath; microwave absorbing material; radome; NMF; IWV; WVR

Email addresses: tong.ning@chalmers.se (T. Ning), kge@chalmers.se (G. Elgered), jmj@chalmers.se (J.M. Johansson)

1. INTRODUCTION

After decades of continuous development, GNSS data have been used successfully in many applications. For example, continuously operating Global Positioning System (GPS) stations have significant advantages for determining the atmospheric Integrated Water Vapour (IWV). The formal uncertainty is in the order of 0.5 kg/m^2 and Root-Mean-Square (RMS) difference seen in comparisons to other instruments, such as radiosondes and microwave radiometers, typically ranges from 1.2 and 2.8 kg/m^2 (*Wang et al.*, 2007). Based on the highly precise orbit information and consistent Earth orientation parameters, the accuracy of horizontal position estimates from the GPS data are at the millimetre level (*Hill et al.*, 2009). However, the characteristic of GNSS also makes it vulnerable to some errors. For example, the GNSS antennas have low directive gain (hemispheric coverage) in order to simultaneously track as many satellites as possible. As a result, site dependent systematic effects, i.e. scattering and multipath reflections of the signal observed at low elevation angles, cannot be neglected. Therefore, this type of error needs to be carefully investigated and mitigated to improve the performance.

Multipath happens when the signals from a satellite are reflected by some reflecting objects, e.g. huts, walls, trees and so on. As a result, the grounded receiver captures the same signal sent by a given satellite from different directions. Since the reflected signals always travel a longer path than the direct one, the superposition of the two types of signals causes errors in the pseudorange measurements. In order to avoid the reflected signals from the positive elevation angle, antennas from continuously operating stations for geodetic measurements are mounted far away from big buildings. In addition, the antennas are equipped with choke ring assembly designed to reject the reflected signals arriving from negative elevation angles. However, most GNSS antennas are required to has low directive gain in order to receive signals from low positive elevation angles. Due to this requirement, the gain of the antenna at the negative elevation angle is too high to completely eliminated the reflected signals from this side.

The effects of multipath on geodetic estimates of the site position have been investigated in previous studies (e.g. *Elósegui et al.*, 1995; *Jaldehag et al.*, 1996). These studies found that the scattering from the reflecting structures within the near-field region (less than a few metres from the antenna), can produce errors of a centimetre or greater in the estimated vertical coordinate, but no significant effects in the horizontal parts. The top surface of the pillar and the metal structures to support the antenna are also possible sources for generating scattering. *King and Watson* (2010) showed that the model of time-constant multipath effects is insufficient applied at many sites, the development of a mitigation approach is therefore highly desirable.

To avoid the accumulation of snow, and for a general protection, many antennas of permanent GPS stations are equipped with radomes. Offsets in the

order of centimetres in the vertical component were found due to the installation a radome on a GNSS antenna (*Williams*, 2003). Different shapes of radomes (mainly conical and hemispherical) yield different impacts on phase of the signal. Investigations of such systematic errors have shown that the hemispherical radome design is preferred to get high accuracy (e.g. *Johansson et al.*, 1998; *Emardson et al.*, 2000).

Here we address the influence of the implementation of microwave absorbing material and a hemispherical radome on the estimates of the relative site coordinates, and the IWV. In Section 2, we describe the two GPS stations involved in this study. In Section 3, different setups of the antenna of the experimental station are presented. The processing of the GPS data is also described. Sections 4 and 5 present results regarding the use of antenna corrections, and impacts of the antenna environment, respectively. The conclusions end the paper in Section 6.

2. EXPERIMENTAL SETUP

During the autumn of 2005, an experimental pillar was constructed for flexible mounting of GNSS antennas over a reference marker, namely ONTE, at the Onsala Space Observatory. A Leica AT504GG antenna was mounted on a circular concrete pillar with a beveled top surface and a height of 1 m (see Figure 1a). The continuously operating IGS station ONSA is 12 m away from the ONTE antenna (see Figure 2a). The ONSA antenna is the Allen Osborne Associates Dorne Margolin B (AOAD/M_B), which is centered in a choke ring assembly and on the top of a 1 m high concrete pillar. A microwave absorber is attached to the antenna and a hemispheric radome is used (see Figure 1b and Figure 2b). During this experiment, the ONTE antenna is always fixed in the centre of the pillar. When the radome is put on the antenna, it is always in the centre with respect to the pillar. The type of the microwave absorbing material used is the ECCOSORB® AN-W 77 with a standard size $61 \times 61 \times 5.7$ cm (see: **http://www.eccosorb.com/products/10**). It is designed to reflect less than -20 dB of normal incident energy with frequencies above 1.2 GHz and is therefore suited for the GPS frequencies (1.23 and 1.58 GHz). An absorbing sheet was put under the antenna ground plane to block the scattering from the top surface of the pillar and the metal plate to support the antenna (see Figure 3b and c). An absorbing ring was also produced to cover the whole circumference of the choke ring to reduce the possible scattering effects from this part (see Figure 3b). All measurements of a certain setup of the antenna were performed twice (with and without the radome). A Water Vapour Radiometer (WVR) was also used to measure the sky emission at two frequencies, 21.0 and 31.4 GHz. The amount of water vapour along the direction of the observation can be inferred from the measured sky emission. *Elgered and Jarlemark* (1998) describe the WVR and the corresponding data analysis. The WVR is mounted 10 m from the ONSA site, and at approximately the same height within 0.5 m (see

Figure 2a). Due to less accuracy in WVR measurements during rainy days, we removed the WVR data points with liquid water content bigger than 0.7 mm in order to control the data quality. The IWV derived from the WVR data was used as an independent data set to evaluate the GPS results.

3. GPS DATA ACQUISITIONS AND ANALYSIS

We first made observations with and without the radome on the ONTE antenna for two continuous sessions (A and B) where no absorber was used. In Session C, the absorber was attached both under and around the antenna covered by the radome. The same setup of the absorber, but without the radome was used in Session D. Two other sessions (E and F) were performed with the absorber put only under the antenna ground plane, with and without the use of the radome, respectively. To investigate the reproducibility of the results, identical setups were implemented twice for most sessions distinguished as A1 and A2, B1 and B2, and so on. Table 1 summarizes the different configurations. Note that there are no changes on the IGS station ONSA during the whole experiment.

The acquired GPS measurements of ionospheric free linear combination (LC) were analyzed by the GIPSY/OASIS II software developed by the Jet Propulsion Laboratory (JPL) (*Webb and Zumberge*, 1993), using the Precise Point Positioning (PPP) processing strategy (*Zumberge et al.*, 1997). The newest version (5.0) of the GIPSY/OASIS was used, which has been released by JPL during 2008. The new version of the GIPSY/OASIS enables the usage of the new GPS orbit and clock products provided from a reprocessing of existing archives (**https:// gipsyoasis.jpl.nasa.gov/gipsy/docs/GipsyUsers AGU2007.pdf**). The zenith wet delay, the values of the propagation delay due to water vapour, was estimated as a random walk process (standard deviation of 1 cm/$\sqrt{\text{h}}$) and updated every 300 s. The Niell Mapping Function (NMF) was used in the process to convert the zenith delay to the slant delay in the direction of the observation (*Niell*, 1996). In order to control the quality of GPS data, we rejected zenith delay with standard deviations greater than 10 mm. A model presented in *Emardson and Derks* (1999) depending on the latitude of the site and the day of the year was used to convert the zenith wet delay both from the GPS and the WVR data to IWV. In this work, the analysis standards comply with the IERS conventions and with current IGS analysis standards (*Dow et al.*, 2009), but including an ocean tide loading model in the process (*Scherneck and Bos*, 2002).

To achieve centimetre or better accuracy in the vertical coordinate estimates, calibrations of the Phase Centre Variations (PCV) of GNSS antennas are necessary (discussed in Section 4). We first compare the results with and without using PCV calibrations. Thereafter, we apply these corrections in all studies of

absorber and radome geometries.

4. ANTENNA PHASE CENTRE VARIATIONS

It is important to note that the multipath effects are mixed with the errors associated with the antenna itself which are mostly due to the antenna PCVs. The phase centre of a GNSS antenna is the reception point to where the measured position is referred. The antenna phase centre, however, is not fixed and varies along with elevation angles of observations. The elevation dependence of the PCV is clearly seen in Figure 4 where a comparison was made in the postfit LC phase residuals obtained with and without implementing PCV corrections in the data processing. The RMS differences given in Figure 4 were referred to the square root of the mean squared deviation of residuals for different elevation angles from zero. Unlike the multipath errors, the antenna PCV has a static behavior and can therefore be calibrated using a absolute phase centre correction model. The model gives mean offsets of the electrical antenna phase centre compared to the physical antenna reference point, as well as PCVs as a function of the elevation angle (*Schmid et al.*, 2007). The new version of GIPSY/OASIS (V5.0) includes absolute calibrations, for most of the existing types of GNSS antennas (**http://xenon.colorado.edu/Release_Notes_5.0.pdf**), and the details about the models can be found in **http://www.ngs.noaa.gov/ANTCAL/**. As shown in Figure 4b, a significant part of the PCV is removed after processing with the corrections. Figure 5 shows comparisons of the mean postfit LC phase residuals for Sessions B, D, and F (all sessions without using the radome) obtained with and without the antenna PCV correction. The comparisons for the sessions with using the radome (A, C, and E) are shown in Figure 6. It is evident from both figures that decreases in the RMS ranging from 1.5 to 1.8 mm are achieved when including the PCV corrections. The results also show that the implementation of the absorber slightly improves the residuals (maximum in 0.3 mm) for all cases, regardless of the correction of the antenna PCV. Insignificant changes in RMS (within 0.3 mm) are seen from the residuals before and after the use of the radome.

5. CASE STUDY OF THE ANTENNA ENVIRONMENT

The impacts of the microwave absorber and the radome are studied from the estimates for the relative coordinates of the baseline and the IWV. The IWV is also compared to the result from the independent WVR data.

5.1. Impacts of the Microwave Absorber

Figure 7 shows the elevation angle dependence in the estimated east, north, and vertical components of the baseline. The detailed values are given in Table 2. Plotted data points are mean offsets relative to the value from the 5° cutoff

angle solution of Session B (no absorber, no radome). The error bars are the standard deviations of the differences. The results demonstrate significant deviations (the maximum is ∼27 mm between the 5° and the 20° solutions) in the vertical components if there is no absorber attached to the antenna (Sessions A and B in Figure 7c and d). As shown in Figure 7a and b, for sessions B, D, and F, no impacts are seen on the horizontal components. Similar results are obtained for sessions A, C, and E (not shown). The implementation of the absorber significantly, but not completely, removes the variations in the vertical with the elevation cutoff angle. The offset between the 5° and the 20° solutions is now decreased to only ∼4 mm from the value of 27 mm. By comparing the results from Sessions C and E, and Sessions D and F, we can see the differences in impact of the absorber with two configurations. As shown in Table 2, no significant differences ($>3\sigma$) are evident. A maximum difference in 5.4 mm is seen from the comparison between Session C and E for the 25° solutions. However, this value is still comparable to the uncertainty of the difference which is around 2.9 mm.

Figure 8 shows the time series of the IWV from October, 2008 to November, 2009, obtained from the WVR data. The comparison results to the GPS data are shown in Figure 9. We averaged the WVR IWV using a window of one hour to match the hourly GPS-estimated IWV, which was transformed from the zenith wet delay using hourly ground pressure measurements. The mean IWV difference and the standard deviation of the difference for each session are also given numerically in Figure 9. On the average for the whole time series, the WVR data are 0.35 kg/m^2 above the ONSA-estimated IWV. High correlations in IWV difference between ONSA-WVR and ONTE-WVR are evident, regardless if we used the absorber on the ONTE antenna. It is also evident that the differences in the IWV between the two GPS data sets decrease for all sessions with the absorber, which is not surprising given that the ONSA station is always equipped with an absorber. The results also show a good consistency in the IWV difference (within 0.15 kg/m^2) between the two GPS stations, where comparing the sessions with identical setup, i.e. Session A1 and A2, B1 and B2, and so on.

Figure 10 shows comparisons of the mean IWV differences given in each session between the WVR and the GPS data, which were obtained from the elevation cutoff angle of 5° to 20°. Significant offsets (∼1.2 kg/m^2 on average) in the mean IWV differences are seen for Sessions A and B (see Figure 10b) from the comparison between the ONTE and the WVR, when the elevation angle varies from 5° to 20°. The offsets drop to around 0.6 kg/m^2 on average for all other sessions with the absorber. Similar offsets (∼0.58 kg/m^2 on average) are seen from the comparison between the ONSA and the WVR for the whole period. The results again indicate that the implementation of the absorber significantly, but not completely, removes the elevation dependent variations. Note in Figure 10b that the tendency of differences is reversed after the use of the absorber (after Session A2). This can be simply due to the absorber somehow

change the character of the multipath effects. However, different weather conditions, e.g. the residence of the water on the absorber plane due to rain, are also possible to cause this change.

Statistics in the IWV difference between the two GPS stations are given in Figure 11 showing the daily mean differences of the IWV obtained using the 15° solution. The offsets in the difference, relative to those obtained without using the absorber are given numerically to demonstrate the impact of the absorber. The results show that significant offsets (0.83 ± 0.23 and 1.09 ± 0.27 kg/m^2) were caused by using the absorber. The offsets slightly change to 0.55 ± 0.33 and 0.94 ± 0.26 kg/m^2 for the sessions with repeated configurations of the absorber, but without the radome on the ONTE antenna (Sessions B, D, and F). The difference in the results from the sessions with the two types of the absorber geometries are small (0.26 and 0.39 kg/m^2, respectively). Figure 12 shows the impact of the implementation of the absorber on the estimated IWV (c.f. Figure 7) for all five different elevation cutoff angles. The IWV results are similar to the ones for the estimated vertical component. By using the absorber, the elevation angle dependent variations in the IWV are significantly reduced, from ∼1.6 kg/m^2 to ∼0.3 kg/m^2. Two different configurations of the absorber give similar results with a mean difference less than 0.25 kg/m^2.

5.2. Impacts of the Radome

We made comparisons on the offsets of the vertical component of the baseline obtained from paired sessions with same configuration, but with and without the radome, i.e. Sessions A/B, C/D, and E/F. The statistics of the comparisons are given in Table 3. The results show no significant offsets ($>3\sigma$) in the vertical component for all session pairs. The offsets for the IWV calculated in the same way as shown in Figure 11, but relative to those obtained with using the radome are given in Figure 13 to demonstrate the impact of the radome. The offsets are all insignificant compared to 1σ. Table 4 presents the changes in IWV offset introduced by the radome, and indicates that no significant impacts were caused by the radome.

6. CONCLUSIONS

We have shown that the elevation angle dependent effects, i.e. scattering and multipath reflections, have significant influence on the estimates of the vertical component of the relative site position. The multipath effects can be significantly reduced by using the microwave absorption material, e.g. ECCOSORB®. The variations in the vertical component significantly drops from ∼27 mm to ∼4 mm when the elevation cutoff angle varies from 5° to 20°. The maximum difference in 5.4 mm, but with a comparable uncertainty in 2.9 mm, is seen from the results with two different configurations of the absorber (only under or both under and around the antenna). Using the absorber also yields significant changes

from ∼1.6 kg/m^2 to ∼0.3 kg/m^2 in the estimate of the atmospheric IWV. A difference less than 0.25 kg/m^2 is seen from the two configurations of the absorber. Comparisons between the WVR and the GPS data give consistent results. A reversed tendency in IWV difference between ONTE and WVR after using the absorber is interesting to see. However, it is hard to explain. In conclude, in order to have a stable and good quality in GNSS measurements regardless unexpected changes from the electromagnetic environment of the ground antenna (e.g. growing trees and the ground changes due to different weather conditions), putting a microwave absorbing material to the antenna in either way discussed in this study is highly recommended.

We also investigated the influence of the installation of a hemispheric radome on the GPS antenna. Small offsets (∼1–3 mm) are caused on the estimates of the vertical component of the baseline for all solutions with elevation cutoff angle of 20° and below. The maximum offset goes up to around 5 mm for 25° solution, but it is still not significant when compared to a relatively large uncertainty of 3 mm. This is similar to the results for the IWV estimates, where no significant deviations ($>3\sigma$ uncertainty) were found. Although the results from this study are only applied to this specific hemispheric radome, which is used for stations in the Swedish network, the insignificant influences of this radome seen from this study shall be interested from other research communities in term of making comparisons to other type of radomes. In addition, these deviations (within 0.4 kg/m^2) may become significant if we are searching for small trends of the IWV. Therefore, all installations and modifications of radomes shall be carefully documented and archived.

The antenna phase centre variations are normally mixed with the multipath effects. By implementing antenna PCV corrections in the GIPSY processing, these errors are significantly reduced.

References

Dow, J.M., Neilan, R.E., Rizos, C., The International GNSS Service in a changing landscape, *J. Geod.*, 83 (3–4), 191–198, 2009.

Elgered, G., Tropospheric radio path delay from ground-based microwave radiometry, *in Atmospheric Remote Sensing By Microwave Radiometry*, 215–258, Wiley & Sons, Inc, 1993.

Elgered, G., Jarlemark, P.O.J., Ground-based microwave radiometry and long-term observations of atmospheric water vapor, *Radio. Sci.*, 33, 707–717, 1998.

Elósegui, P., Davis, J.L., Jaldehag, R.T.K., et al., Geodesy using the Global Positioning System: the effects of signal scattering on estimates of site position, *J. Geophys. Res.*, 100, B6, 9921–9934, 1995.

Emardson, T.R., Derks, H.J.P., On the relation between the wet delay and the integrated precipitable water vapour in the European atmosphere, *Meteorol. Appl.*, 6, 1–12, 1999.

Hill, E.M., Davis, J.L., Elósegui, P., et al., Characterization of site-specific GPS errors using a short-baseline network of braced monuments at Yucca Mountain, southern Nevada, *J. Geophys. Res.*, 114, B11402, doi:10.1029/2008JB006027., 2009.

Emardson, T.R., Johansson, J.M., Elgered, G., The systematic behavior of water vapor estimates using four years of GPS observations, *Trans. IEEE Geosci. Remote Sens.*, 38, 324–329, 2000.

Jaldehag, R.T.K., Johansson, J.M., Rönnäng, B.O., et al., Geodesy using the Swedish permanent GPS network: effects of signal scattering on estimates of relative site positions, *J. Geophys. Res.*, 101, B8, 841–860, 1996.

Johansson, J.M., Emardson, T.R., Jarlemark, P.O.J., et al., The atmospheric influence on the results from the Swedish GPS network, *Phys. Chem. Earth.*, 23, 107–112, 1998.

King, M.A., Watson, C.S., Long GPS coordinate time series: multipath and geometry effects, *J. Geophys. Res.*, in press, 2010.

Niell, A., Global mapping functions for the atmosphere delay at radio wavelengths, *J. Geophys. Res.*, 101, 3227–3246, 1996.

Scherneck, H.-G., Bos, M.S., Ocean tide and atmospheric loading, *Proc. IVS*, 205–214, 2002.

Schmid, R., Steigenberger, P., Gendt, G., et al., Generation of consistent absolute phase-center correction model for GPS receiver and antennas, *J. Geod.*, 81 (12), 781–798, 2007.

Wang, J.H., Zhang, L.Y., Dai, A.G., et al., A near-global, 2-hourly data set of atmospheric precipitable water from ground-based GPS measurement, *J. Geophys. Res.*, 112, doi: 10.1029/2006JD007529, 2007.

Webb, F.H., Zumberge, J.F., An introduction to the GIPSY/OASIS-II, *JPL Publ.*, 1993.

Williams, S.D.P., Offsets in Global Positioning System time series, *J. Geophys. Res.*, 108 (B6), 2310, doi:10.1029/2002JB002156, 2003.

Zumberge, J.F., Heflin, M.B., Jefferson, D.C., et al., GPS Trends in Precise Terrestrial, Airborne, and Spaceborn Applications, *J. Geophys. Res.*, 102, 5005–5017, 1997.

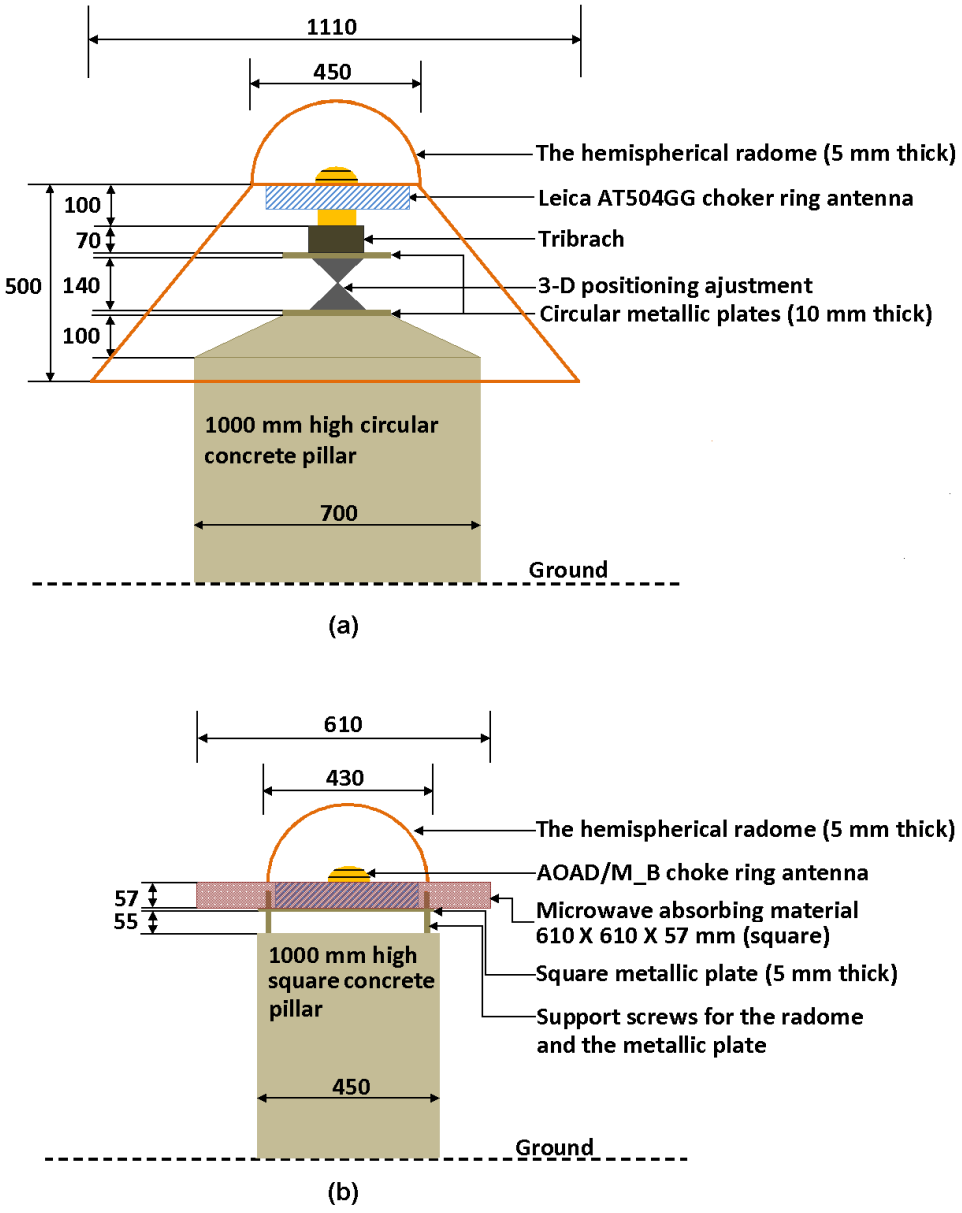

Figure 1: Sketch of (a) the experimental station and (b) the GPS station ONSA. All scales are given in millimetres.

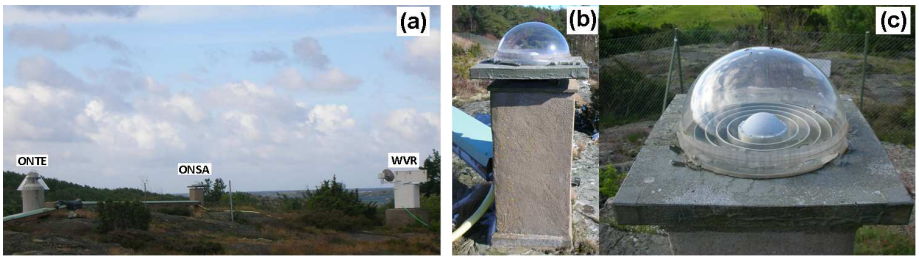

Figure 2: (a) The baseline between the two GPS stations ONTE and ONSA, and the WVR. (b) and (c) The GPS station ONSA with a hemispheric radome and a microwave absorber.

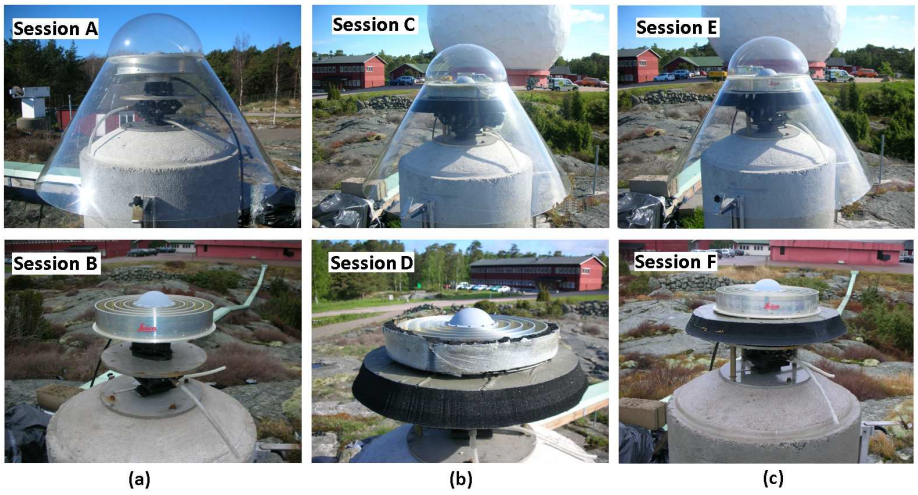

Figure 3: Photographs of the experimental station (ONTE) with (top) and without (bottom) the radome having, (a) no absorber, (b) the absorber attached both under and around the antenna, and (c) the absorber attached only under the antenna ground plane. The sessions are further described in Section 3 and Table 1.

Table 1: The different observing sessions of the experimental station ONTE

Sessions	Configuration of the antenna	Start	End	Days of data set[1]	Figures
A1	With radome, no absorber	2008/10/15	2008/11/17	32	1a (top)
B1	No radome, no absorber	2008/11/17	2008/12/23	26	1a (bottom)
B2	No radome, no absorber	2009/03/20	2009/04/02	12	1a (bottom)
A2	With radome, no absorber	2009/04/02	2009/04/14	7	1a (top)
C1	With radome, with absorber put under and around the antenna	2009/04/30	2009/05/18	16	1b (top)
D1	No radome, with absorber put under and around the antenna	2009/05/26	2009/06/08	12	1b (bottom)
E	With radome, with absorber put under the antenna only	2009/06/08	2009/08/28	64	1c (top)
D2	No radome, with absorber put under and around the antenna	2009/09/22	2009/10/05	12	1b (bottom)
C2	With radome, with absorber put under and around the antenna	2009/10/05	2009/10/18	12	1b (top)
F	No radome, with absorber put under the antenna only	2009/10/18	2009/11/22	33	1c (bottom)

[1]When the configuration was changed or when data were partly missing, data from the entire day were ignored.

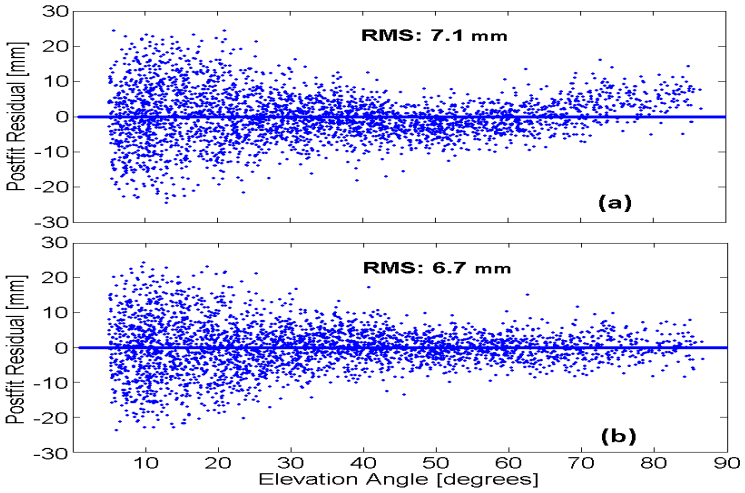

Figure 4: Postfit LC phase residuals from the experimental site (ONTE) for all satellites obtained from the processing (a) without the antenna PCV correction and (b) with the antenna PCV correction. The data set was acquired on October 25th, 2009 (Session F).

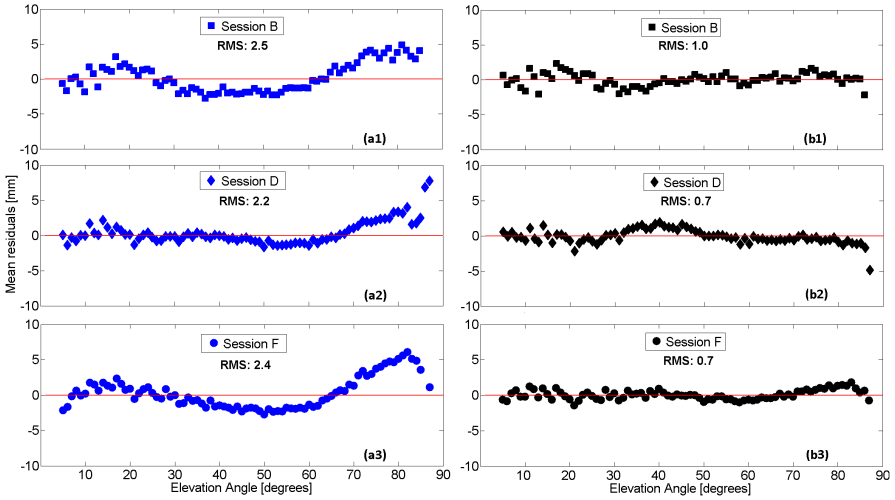

Figure 5: Comparisons of the mean Postfit LC phase residuals from the experimental site (ONTE) for all satellites obtained (a) without the antenna PCV correction and (b) with the antenna PCV correction for Sessions B, D, and F (all sessions without using the radome). Twenty days of data set were included from each session, and the mean was obtained by averaging the residuals for 1 degree intervals.

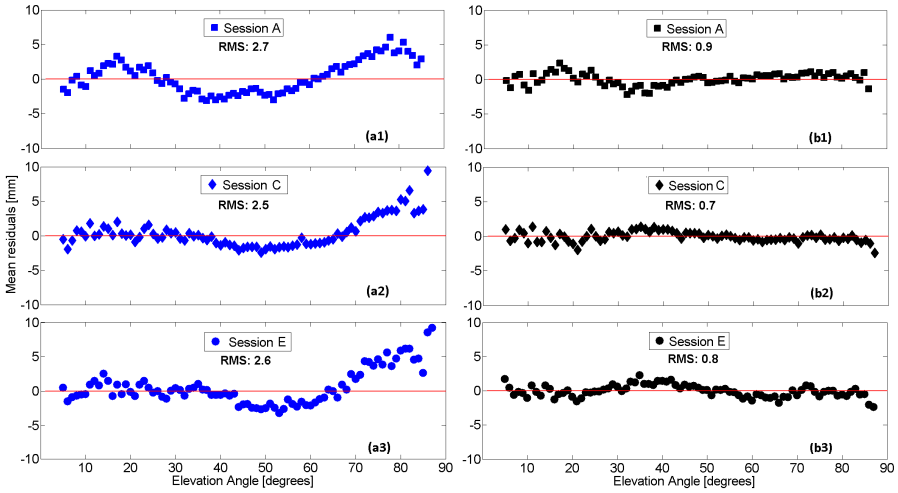

Figure 6: Same as Figure 5, except for Sessions A, C, and E (all sessions with using the radome).

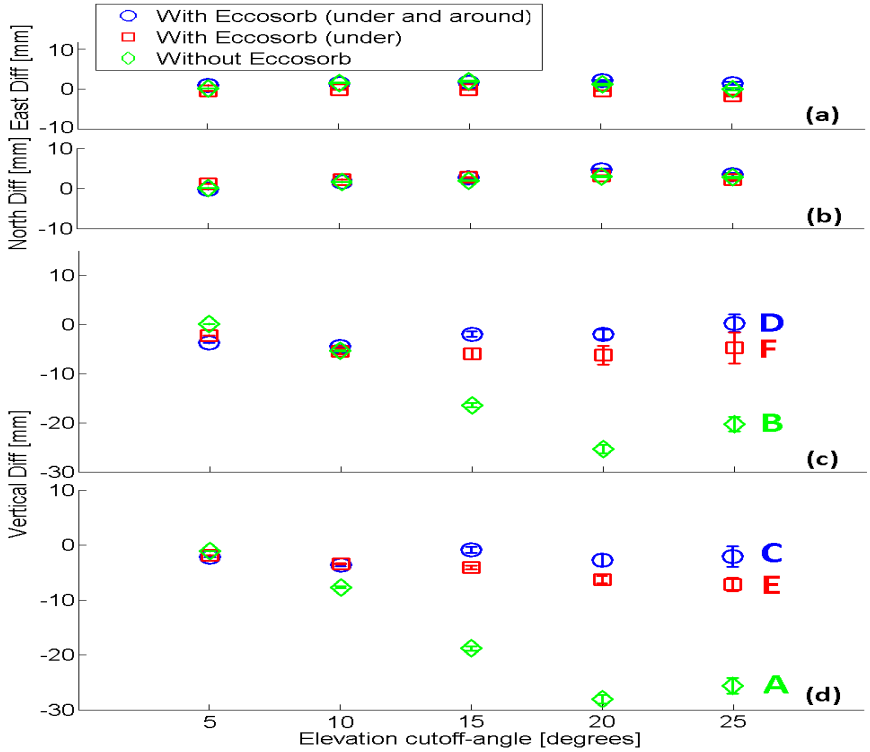

Figure 7: The impact of the elevation cutoff angle on the estimated (a) east, (b) north, (c) vertical components of the baseline without the radome (Sessions B, D, F) and (d) vertical components of the baseline with the radome (Sessions A, C, E).

Table 2: Offsets in the estimated vertical component of the ONSA-ONTE baseline obtained for each session and for all elevation cutoff angle solutions.

Elevation cutoff angle	Offset in the vertical component [mm]					
	Session A	Session C	Session E	Session B	Session D	Session F
5°	−1.0±0.4	−2.1±0.6	−1.7±0.4	0±0	−3.9±0.5	−2.4±0.6
10°	−7.5±0.6	−3.5±0.8	−3.3±0.5	−5.5±0.6	−4.6±0.7	−5.6±0.8
15°	−18.6±0.9	−0.7±1.1	−4.0±0.7	−16.5±0.9	−2.1±1.1	−6.2±1.2
20°	−27.8±1.2	−2.6±1.6	−7.1±1.1	−25.5±1.3	−2.1±1.6	−6.3±1.8
25°	−25.4±1.9	−1.9±2.4	−7.3±1.6	−20.5±1.9	0.1±2.3	−4.2±2.6

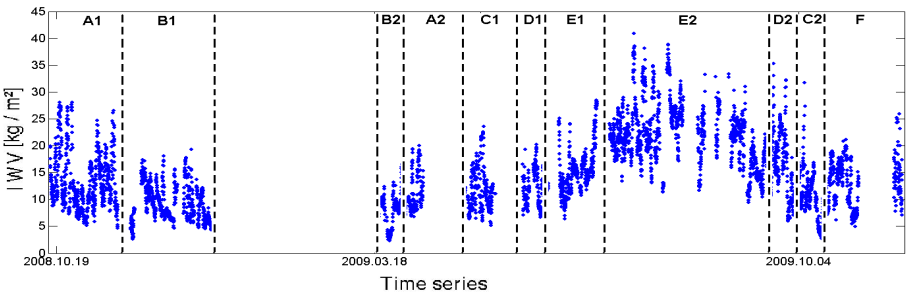

Figure 8: IWV obtained from the WVR data with an elevation cutoff angle of 18°.

Table 3: Offsets in the estimated vertical component of the ONSA-ONTE baseline obtained with and without the radome for all elevation cutoff angle solutions (derived from Table 2).

Elevation cutoff angle	Offset in the vertical component [mm]		
	Session (B−A)	Session (D−C)	Session (F−E)
5°	1.0±0.6	−1.8±0.8	−0.7±0.7
10°	2.1±0.9	−1.1±1.1	−2.3±1.1
15°	2.1±1.2	−1.4±1.5	−2.2±1.5
20°	2.3±1.8	0.5±2.3	0.8±2.2
25°	4.9±2.7	2.1±3.4	3.1±3.3

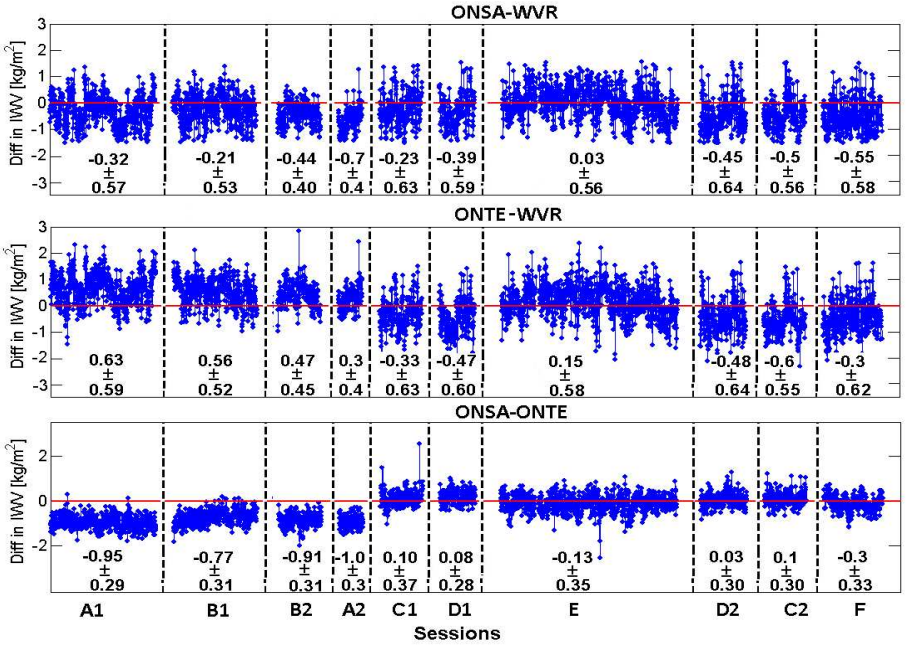

Figure 9: IWV differences with the GPS estimates obtained using an elevation cutoff angle of 15°. Offsets are given for each session relative to the overall mean. The mean IWV difference and the standard deviation of the difference are given numerically for each session.

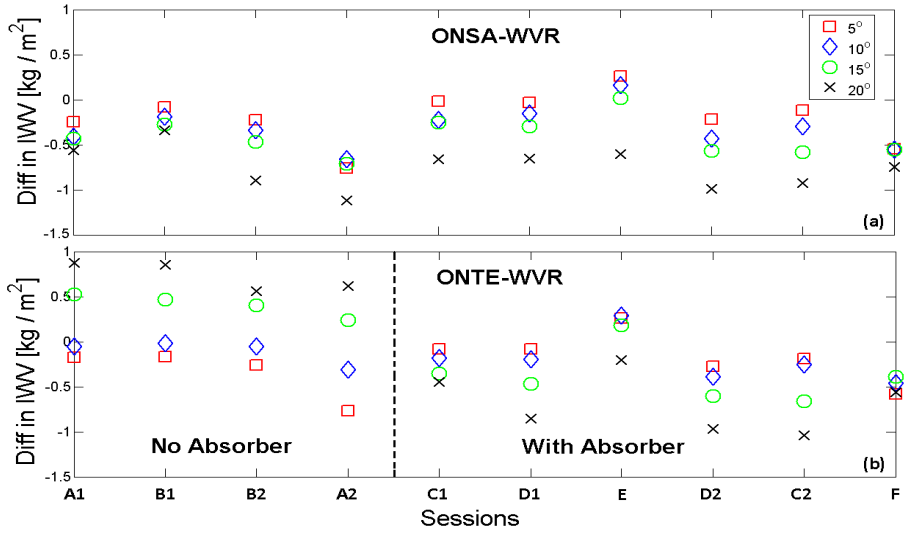

Figure 10: Mean differences in IWV for each session, (a) between the ONSA and the WVR data (b) between the ONTE and the WVR data, from 5° to 20° elevation cutoff angle solutions. The order of the sessions follows the time of the observations.

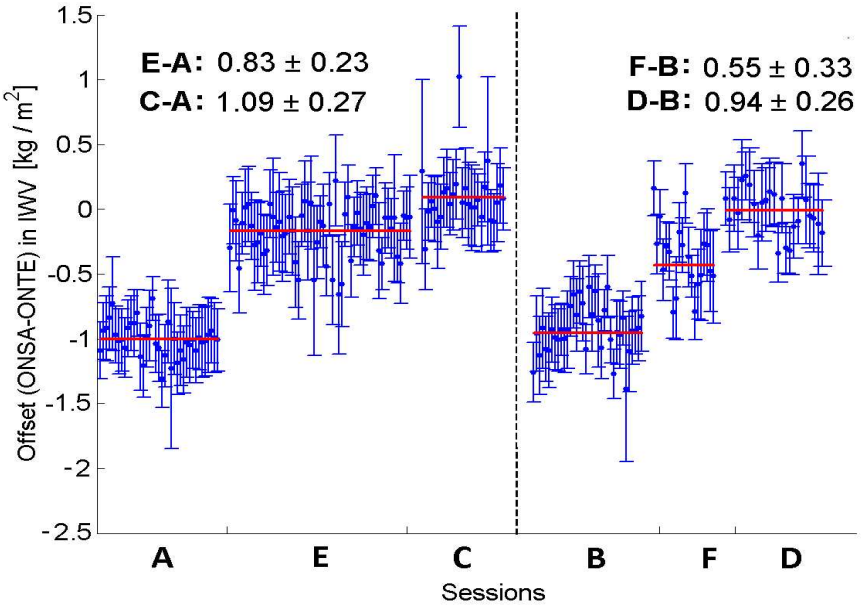

Figure 11: Daily statistics of the IWV for the comparison between two GPS stations. The dots indicate the daily difference and the error bars represent the standard deviation of the difference of the mean for each day. The mean value of each session is shown by solid lines. The estimates are obtained using an elevation cutoff angle of 15°. Differential offsets between pairs of sessions are given numerically (kg/m^2)

Table 4: Same as Table 3 except here for the estimated IWV difference from the two GPS stations, the uncertainties are the standard deviations of the differences.

Elevation	Offset in the IWV difference (ONSA-ONTE) [kg/m^2]					
cutoff angle[1]	Session (B−A)	%[2]	Session (D−C)	%[2]	Session (F−E)	%[2]
5°	0.11±0.16	1.0	−0.01±0.21	0.1	−0.01±0.25	0.1
10°	0.13±0.24	1.2	0.02±0.23	0.2	−0.11±0.27	0.7
15°	0.16±0.28	1.5	−0.03±0.31	0.2	−0.12±0.33	0.7
20°	0.20±0.39	1.9	0.16±0.4	1.4	0.04±0.45	0.1
25°	0.38±0.46	3.7	0.3±0.46	2.8	0.14±0.57	0.8

[1]The results for 15° are also shown in Figure 13.
[2]The percentage of IWV difference of the mean value of the two sessions in the comparison.

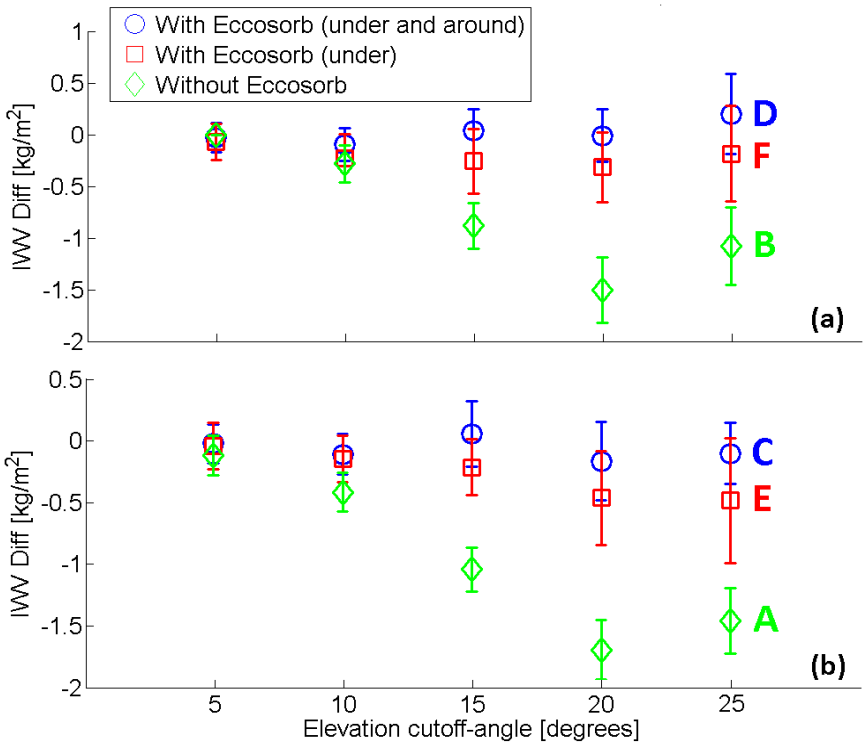

Figure 12: Same as Figure 7 but here for the IWV difference between the two GPS stations.

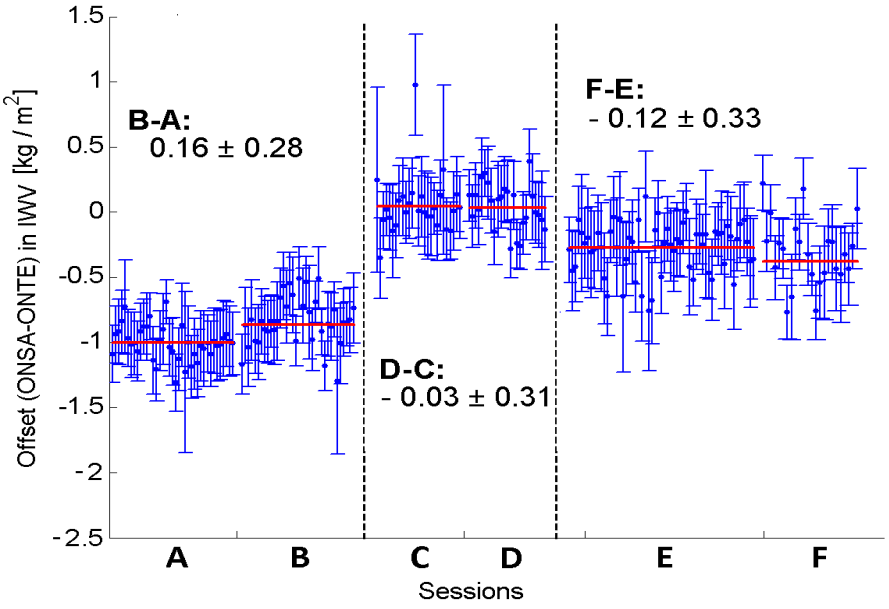

Figure 13: Same as Figure 11, but rearranged to show the impacts of the usage of the radome.